

NLRP3 inflammasome activation in sensory neurons promotes chronic inflammatory and osteoarthritis pain

Patrícia Silva Santos Ribeiro^{id}, Hanneke L.D.M. Willemen^{id}, Sabine Versteeg,
Christian Martin Gil and Niels Eijkelkamp^{*id}

Center for Translational Immunology, University Medical Center Utrecht, Utrecht University, Utrecht, The Netherlands

*Correspondence: Center for Translational Immunology, University Medical Center Utrecht, Utrecht University, Lundlaan 6, 3584 EA Utrecht, The Netherlands.
Email: N.Eijkelkamp@umcutrecht.nl

Summary

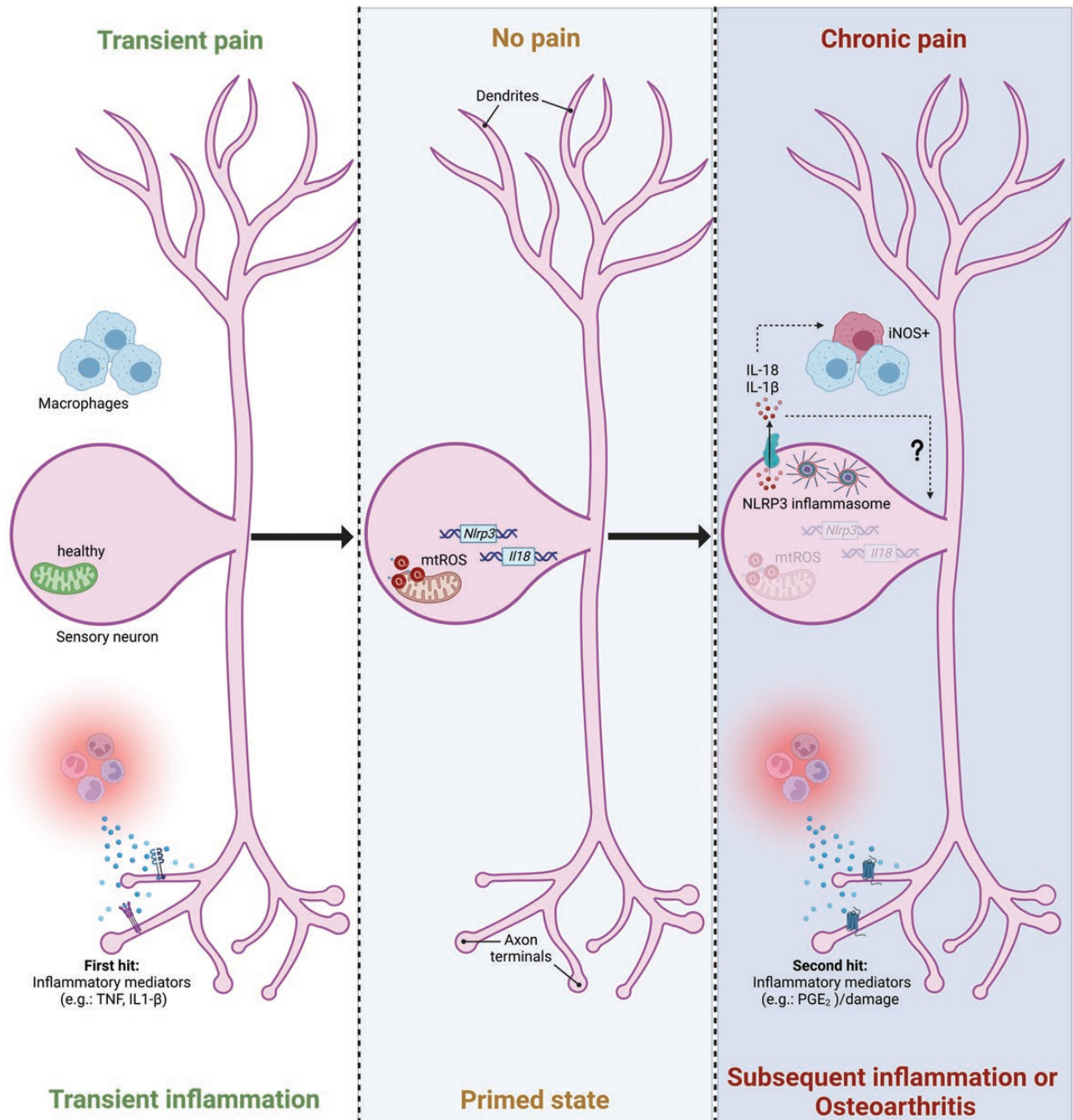
Pain is one of the most debilitating symptoms in rheumatic diseases. Pain often persists after total knee replacement in osteoarthritis, or when inflammation is minimal/absent in rheumatoid arthritis. This suggests that pain transitions to a chronic state independent of the original damage/inflammation. Mitochondrial dysfunction in the nervous system promotes chronic pain and is linked to NLRP3 inflammasome activation. Therefore, we investigated the role of mitochondrial dysfunction and NLRP3 inflammasome activation in the transition from acute to persistent inflammation-induced nociceptive pain and in persistent monoiodoacetate-induced osteoarthritis pain. Intraplantar injection of carrageenan in mice induced transient inflammatory pain that resolved within 7 days. A subsequent intraplantar PGE₂ injection induced persistent mechanical hypersensitivity, while in naive mice it resolved within one day. Thus, this initial transient inflammation induced maladaptive nociceptor neuroplasticity, so-called hyperalgesic priming. At Day 7, when mice were primed, expression of NLRP3 inflammasome pathway components was increased, and dorsal root ganglia (DRG) neurons displayed signs of activated NLRP3 inflammasome. Inhibition of NLRP3 inflammasome with MCC950 prevented the transition from acute to chronic pain in this hyperalgesic priming model. In mice with persistent monoiodoacetate-induced osteoarthritis pain, DRG neurons displayed signs of mitochondrial oxidative stress and NLRP3 inflammasome activation. Blocking NLRP3 inflammasome activity attenuated established osteoarthritis pain. In males, NLRP3 inhibition had longer-lasting effects than in females. Overall, these data suggest that NLRP3 inflammasome activation in sensory neurons, potentially caused by neuronal oxidative stress, promotes development of persistent inflammatory and osteoarthritis pain. Therefore, targeting NLRP3 inflammasome pathway may be a promising approach to treat chronic pain.

Received: April 3, 2023; Accepted: October 23, 2023

© The Author(s) 2023. Published by Oxford University Press on behalf of the British Society for Immunology.

This is an Open Access article distributed under the terms of the Creative Commons Attribution-NonCommercial License (<https://creativecommons.org/licenses/by-nc/4.0/>), which permits non-commercial re-use, distribution, and reproduction in any medium, provided the original work is properly cited. For commercial re-use, please contact journals.permissions@oup.com

Graphical Abstract



Keywords: chronic pain, osteoarthritis, NLRP3 inflammasome, sensory neurons, mitochondrial dysfunction, hyperalgesic priming

Abbreviations: 18S: Ribosomal RNA 18S; 3D: Three dimensional; ASC: Apoptosis-associated speck-like protein containing a CARD; ATP: Adenosine triphosphate; ATPSc-KMT: ATP Synthase C Subunit Lysine N-Methyltransferase; CARD: Caspase activation and recruitment domain; CD11b: Cluster of differentiation molecule 11b; CD115: Cluster of differentiation 115; CD163: Cluster of differentiation 163; CD16/CD32: Cluster of differentiation 16/32; CD206: Cluster of differentiation 206; CD45: Cluster of differentiation 45; cDNA: Complementary deoxyribonucleic acid; COVID: Corona virus disease; CT: Cycle threshold; DAPI: 4',6-diamidino-2-phenylindole; DMEM: Dulbecco's modified Eagle medium; DRG: Dorsal root ganglia; ECAR: Extracellular acidification rate; EDTA: Ethylenediaminetetra acetic acid; FACS: Fluorescence activated cell sorting; FCCP: Carbonyl cyanide-p-trifluoromethoxyphenylhydrazone; HBSS: Hank's Balanced Salt Solution; HEPES: 4-(2-hydroxyethyl)-1-piperazineethanesulfonic acid; i.p.: Intraperitoneal; i.t.: Intrathecal; IL-18: Interleukin 18; IL-1β: Interleukin 1β; IL-6: Interleukin 6; iNOS: Inducible nitric oxide synthase; LRR: Leucine-rich repeats; Ly6G: Lymphocyte antigen 6 family member G; MFI: Mean fluorescence intensity; MIA: Monoiodoacetate; mRNA: Messenger ribonucleic acid; mtDNA: Mitochondrial deoxyribonucleic acid; mtROS: Mitochondrial reactive oxygen species; N/A: Not applicable; NA: Numerical aperture; NaCl: Sodium Chloride; NADPH: Nicotinamide adenine dinucleotide phosphate oxidase; NLRP3: NOD-, LRR- and pyrin domain-containing protein 3; NOD: Nucleotide-binding oligomerization domain; NOX2: NADPH oxidase 2; OA: Osteoarthritis; OCR: Oxygen consumption rates; PBS: Phosphate-buffered saline; PCR: Polymerase chain reaction; PFA: Paraformaldehyde; PGE₂: Prostaglandin E₂; RA: Rheumatoid arthritis; RNA: Ribonucleic acid; ROS: Reactive oxygen species; RT-qPCR: Real time quantitative PCR; SD: Standard Deviation; SEM: Standard error of the mean; SSC: Side scatter; TLR4: Toll-like receptor 4; TNF: Tumor necrosis factor; Tris-HCl: Tris(hydroxymethyl)aminomethane hydrochloride; UMAP: Uniform Manifold Approximation and Projection.

Introduction

Pain, caused by joint damage or inflammation, is one of the major symptoms in osteoarthritis (OA) or rheumatoid arthritis (RA) [1, 2]. Intriguingly, pain persists in 10–40% of the OA patients when the joint has been replaced [3]. Similarly, in 12–70% of RA patients, pain persists even when inflammation is absent or minimal [4, 5]. These data suggest that in these patients, pain does not resolve even when the initial inflammatory or damage triggers have disappeared. Current treatments, including non-steroidal anti-inflammatory drugs, steroids, or opioids, are not effective in treating this chronic pain. As example, opioids only reduce pain intensity for ~10% in 20–30% of OA patients [6]. Until now, the mechanisms that cause the switch from acute to chronic pain after inflammation or joint damage remain elusive.

Mitochondria are indispensable for neuronal functioning, and accumulating evidence suggests mitochondrial dysfunction, including reactive oxygen species (ROS) production, is linked to neuronal sensitization and chronic pain development [7–14]. For example, a transient inflammation causes an increase in mitochondrial respiration and mitochondrial ROS (mtROS) production in dorsal root ganglia (DRG) neurons that innervate the inflamed paw. This elevated mtROS persists beyond resolution of this inflammatory pain [15], and contributes to the switch from acute to chronic pain after a second inflammatory stimulus [16]. Moreover, some evidence suggests that oxidative stress and/or decreased antioxidants contribute to pain in OA [17]. However, how mtROS may promote chronic pain is not clear.

Oxidative stress is a known trigger for the activation of the NOD-, LRR-, and pyrin domain-containing protein 3 (NLRP3) inflammasome. The current view is that canonical activation of NLRP3 inflammasome occurs in a two-step process. A first stimulus, e.g. lipopolysaccharides, TNF, IL-1 β , increases the expression of *NLRP3*, *pro-IL-1 β* and *pro-IL-18*. A second stimulus, e.g. ROS, mtDNA, extracellular ATP, induces the assembly and activation of the NLRP3 inflammasome multiproteic complex. NLRP3 engages with pro-caspase-1 through adapter molecule apoptosis-associated speck-like protein containing a CARD (ASC). As a consequence, activated caspase-1 catalyzes proteolytic cleavage of precursors of IL-1 β and IL-18 into their mature forms [18–20]. These downstream cytokines are known to contribute pain; IL-1 β induces action potential firing of sensory neurons, increases their excitability and induces pain [21]. Similarly, IL-18 is involved in various experimental chronic pain conditions [22–24]. Given the evidence that mtROS promotes chronic pain and mtROS may promote NLRP3 inflammasome activation [15], we determined if mitochondrial dysfunction in sensory neurons promotes the transition from acute to chronic pain via NLRP3 inflammasome activation.

Materials and methods

Animals

Adult male and female (7–16 weeks) C57BL/6 mice (Janvier Laboratories) were used for all experiments. Mice were maintained in the animal facility of the University of Utrecht, housed in groups, under a 12 h:12 h light/dark cycle. Food and water were provided *ad libitum*. The cages contained environmental enrichment comprising tissue papers and plastic/paper shelters. Involved experimenters were blinded for the

treatments. G*Power version 3.1 [25] was used to calculate the number of mice per group needed prior to the execution of experiments. All experiments were performed in accordance with international guidelines and approved by the local experimental animal welfare body and the Dutch Central Authority for Scientific Procedures on Animals (AVD115002015323 and AVD11500202010805).

Hyperalgesic priming model

Mice received an intraplantar injection of 5 μ l λ -carrageenan (1% w/v in saline, Sigma-Aldrich) to induce hyperalgesic priming. Non-primed mice received the same volume of sterile saline solution (sodium chloride 0.9% w/v, Fresenius Kabi Nederland BV). At Day 7 after carrageenan or saline, mice received an intraplantar injection of PGE₂ (Sigma Aldrich). PGE₂ was diluted in saline and injected as 2.5 μ l to inject 100 ng/paw (stock solution: 2.5 μ g/ μ l dissolved in ethanol).

Murine OA model

Mice received an intra-articular injection of 10 μ l monoiodoacetate (MIA 10% w/v; Sigma-Aldrich) in one knee (ipsilateral side) under isoflurane anesthesia. The other knee was injected with 10 μ l sterile saline solution (sodium chloride 0.9% w/v). Knee joints were positioned at a 90° angle to perform the injections with a 30G needle coupled to a Hamilton syringe [26, 27].

Drugs

MCC950 (Sigma-Aldrich) was injected either via intraperitoneal (10 mg/kg) or intrathecal injection (5 μ M in saline solution, 5 μ l per animal). The control group received the same volume of sterile saline solution (sodium chloride 0.9% w/v). Intrathecal injections were performed under light isoflurane anesthesia [28].

Behavioral tests

Mice were acclimatized to the experimental setup at least one week prior to the beginning of each experiment. Two to three baseline measurements were acquired for each behavioral test. The average baseline mechanical thresholds were used to randomly assign the mice to the different groups using RandoMice v1.1.1 [29]. Mechanical hyperalgesia was determined using the von Frey test (Stoelting) with the up-and-down method previously described to determine the 50% threshold [30]. In short, von Frey filaments were applied for a maximum of 5 s to the plantar surface of the paw. If the first filament (0.4 \times g) did not produce a response (paw licking or flicking), the subsequent filament with a higher force was applied. If there was a response, the next lower force filament was applied. Weight bearing changes were assessed using the dynamic weight-bearing device (Bioseb). The parameters for analysis were (i) low-weight threshold of 0.5 g, (ii) high-weight threshold of 1 g, (iii) surface threshold of two cells, and (iv) minimum of five images (0.5 s) for stable segment detections [31]. Results are expressed as the ratio between the weight placed on the ipsilateral paw and the weight placed on the contralateral paw. Each animal was considered as an independent experimental unit.

Seahorse measurements

Lumbar (L3-L5) DRG were collected from mice to measure mitochondrial respiration in sensory neurons. Tissues were gently minced and digested at 37°C for 30 min using an

Table 1. Primers used for RT-qPCR

Target	Forward	Reverse
NLRP3	AgAAgAgACCACggCAgAAg	CCTTggACCaggTTCagTgT
IL-18	CAAACCTTCCAAATCACTTCCT	TCCTTgAAgTTgACgCAAgA
IL-1 β	CAACCAACAAgTgATATTCTCCATg	gATCCCACTCTCCAgCTgCA
IL-6	TCTAATTCATATCTTCAACCAAgAgg	TggTCCTTAgCCACTCCTTC
18S	gTAACCCgTTgAACCCCAT	CCATCCAATCggTAgTAgCg
B2M	ATTCACCCCACTgAgACTg	TgCTATTTCTTTCTgCgTgC
TBP	CCTTgTACCCTTCACCAATgAC	ACAgCCAAgATTCACggTAgA
Rictor	TgCgATATTggCCATAgTgA	ACCCggCTgCTCTTACTTCT

enzyme cocktail containing 5 mg/mL collagenase type XI (Sigma-Aldrich) and 10 mg/mL dispase (Gibco™ Thermo Fisher Scientific), solved in Ca²⁺- and Mg²⁺-free HBSS (Gibco™ Thermo Fisher Scientific) with 5 mM HEPES (Gibco™ Thermo Fisher Scientific) and 10 mM glucose (Sigma-Aldrich), to obtain a single cell suspension. Cells were seeded on poly-D-ornithine/laminin (Sigma-Aldrich) coated XF24 wells plates (Agilent Technologies) and rested overnight at 37°C 5% CO₂ in Dulbecco's modified Eagle medium (DMEM) (1×) + GlutaMAX™-I (Gibco™ Thermo Fisher Scientific) containing 10% fetal bovine serum (Invitrogen™ Thermo Fisher Scientific) and 1% Penicillin/Streptomycin (Invitrogen™ Thermo Fisher Scientific). The following day, cells were washed and placed in Seahorse XF-assay media (pH 7.4, Agilent Technologies) containing 25 mM glucose (Sigma-Aldrich), 4 mM glutamine (Sigma-Aldrich), and 1 mM pyruvate (Lonza) at 37°C for 1 h. Oxygen consumption rate (OCR) and extracellular acidification rate (ECAR) were measured using the Seahorse Bioscience XFe24 Analyzer (Seahorse Bioscience). After assessing basal OCR, 2 μ M oligomycin (Cayman Chemicals), 2 μ M FCCP (Sigma-Aldrich) and 2 μ M of Rotenone (Sigma-Aldrich) and Antimycin A (Sigma-Aldrich) were injected after cycle 3, 6, and 9, respectively. Each cycle comprehended 1.5-min of mixing, 2 min waiting, and 3 min of measurements. For each condition (basal, oligomycin, FCCP, rotenone + antimycin A), three cycles were used. Measurements were normalized for protein content.

Measurement of mitochondrial respiration in sciatic nerves was performed according to Krukowski *et al.* [32]. Sciatic nerves were isolated and stored in Seahorse XF media on ice for transport. Subsequently, sciatic nerves were placed into islet capture XF24 microplates (Agilent Technologies) containing Seahorse XF-assay media supplemented with 5.5 mM glucose (Sigma-Aldrich), 0.5 mM sodium pyruvate (Sigma-Aldrich), and 1 mM glutamine (pH 7.4, Sigma-Aldrich). Plates were settled for 2 h at 37°C with 0% CO₂ to degas. OCR and ECAR levels were measured under basal conditions, and after sequential addition of 12 μ M oligomycin, 20 μ M FCCP, and 20 μ M antimycin A and 20 μ M Rotenone [32]. Each cycle comprehended 3 min of mixing, 3 min waiting, and 4 min of measurements.

After the Seahorse measurements, the cells or nerves in each well (one nerve per well) were collected for protein quantification in a lysis buffer containing 20 mM Tris-HCl (Sigma-Aldrich), 137 mM NaCl (Sigma-Aldrich), 2 mM EDTA (Sigma-Aldrich), and 1% v/v Triton X-100 (Merck Millipore). The sciatic nerves were sonicated, centrifuged and

protein concentrations of the lysates were determined using a Bradford assay (Bio-Rad). Measurements were normalized for protein content.

Mitochondrial ROS detection

MitoTracker™ Red CM-H2Xros (Invitrogen™ Thermo Fisher Scientific), which emits fluorescence upon oxidation by mitochondrial reactive oxygen species (mtROS) [33], was injected via intrathecal injection (10 μ l of 100 μ M). Six hours later mice were perfused with phosphate-buffered saline (PBS) and 4% paraformaldehyde (PFA, VWR) under anesthesia. Lumbar (L3-L5) DRG were isolated, cryoprotected in sucrose (30% w/v in PBS, Sigma-Aldrich), embedded and frozen in optimal cutting temperature compound (Tissue-Tek, Sakura). DRG were cut in 10 μ m thick cryosections using a cryostat (CM 3050S, Leica) and collected on SuperFrost plus microscope slides (VWR International). Cryosections were stained with NeuroTrace™ 435/455 (1:300, Thermo Fisher Scientific) to visualize the neurons.

Fluorescence was captured using Olympus IX83 microscope (Olympus) and analyzed with ImageJ software. Two or three pictures of each DRG were acquired. Based on the NeuroTrace™ signal, regions of interest were selected manually, so MitoTracker™ Red CM-H2Xros mean fluorescence intensity (MFI) could be measured in those regions that correspond to the soma of sensory neurons. MFI was corrected by subtracting the background MFI in each picture. A neuron was defined as positive if MFI was higher than the mean + 2SD of DRG neurons of control mice (Day 0 after MIA). The number of positive neurons was expressed as a percentage of the total number of neurons in each picture. Fluorescence was analyzed in small diameter neurons (< 20 μ m) and medium/large diameter neurons (> 20 μ m).

Real-time (RT)-qPCR

RNA was isolated from total lumbar (L3-L5) DRG using TRIzol™ (Thermo Fisher Scientific) and the RNeasy mini kit (Qiagen). cDNA was synthesized using iScript reverse transcription supermix, according to the manufacturer's protocol (Bio-Rad AbD Serotec GmbH). Quantitative real-time PCR reaction was performed with a QuantStudio 3 (Thermo Fisher Scientific) using the following primers (Table 1):

mRNA expression is calculated as $relative\ expression = 2^{C_T(average\ of\ reference\ genes) - C_T(target)}$. We used the average of 18S and B2M as reference for the OA model and 18S, TBP and Rictor as reference for the hyperalgesic priming model.

Table 2. Antibodies used for flow cytometry

Target	Clone	Fluorophore	Dilution	Supplier	Catalog #
Fixable Viability Dye eFluor 506	N/A	BV-510	1:1000	Invitrogen eBioscience	15560607
CD45	30-F11	APC-ef780	1:600	eBioscience	47-0451-80
CD11b	M1/70	PerCP-Cy5.5	1:600	BioLegend	101227(8)
F4/80	BM8	FITC	1:600	BioLegend	123108
Ly6G	1A8	BV-785-A	1:300	BioLegend	127645
Inos	CXNFT	APC	1:240	eBioscience	17-5920-80
CD163	TNKUPJ	PECy7	1:80	Invitrogen	25-1631-82
CD206	C068C2	BV650	1:120	BioLegend	141723
CD115	AFS98	YeGe2	1:600	eBioscience	61-1152-80
Egr2	erongr2	PE	1:80	eBioscience	12-6691-82

Quantification of NLRP3 inflammasome activation

DRG sections and single cell suspension of DRG neurons were obtained as described above. DRG neuronal cultures were seeded in glass coverslips previously coated with 0.01 mg/mL poly-L-lysine (Sigma-Aldrich) and laminin (Sigma-Aldrich), and rested overnight at 37°C 5% CO₂ in the culture medium previously described. The following day, neuronal cultures were pre-treated with 1 μM MCC950 (Sigma-Aldrich), 500 nM mitoTEMPOL (Cayman Chemical Company), or vehicle for 1 h, followed by 1 or 6 h stimulation with a mixture consisting of 50 ng/mL recombinant mouse IL-1β (BioLegend Europe BV) and 100 ng/mL TNF (PeproTech). When performing experiments with mitoTEMPOL, the culture medium was replaced by HBSS without phenol (Gibco™ Thermo Fisher Scientific) containing 5% fetal bovine serum (Invitrogen™ Thermo Fisher Scientific), 1% Penicillin/Streptomycin (Invitrogen™ Thermo Fisher Scientific), 3.97 mM L-glutamine (Gibco™ Thermo Fisher Scientific), and 25 mM D-(+)-glucose (Gibco™ Thermo Fisher Scientific). After stimulation, the conditioned media was collected and primary neurons were washed for 5 min with PBS (Sigma-Aldrich), fixed in 4% PFA (VWR) for 10 min, and washed with PBS for 5 min.

To determine the concentration of IL-18 in the supernatant of the DRG neuronal cultures, a mouse IL-18 ELISA kit (Medical & Biological Laboratories [MBL]) was used according to the manufacturer's instructions.

For the ASC staining, cells were blocked with 5% normal donkey serum (Jackson ImmunoResearch), 5% normal goat serum (Abcam) and 2% bovine serum albumin (BSA; Sigma-Aldrich) in PBS (Merck Milipore) with 0.05% Tween-20 (Merck Milipore). DRG sections were blocked with 5% normal donkey serum and 5% bovine serum albumin in PBS with 0.05% Tween-20 (Merck Milipore) and 0.1% Triton X-100 (Merck Milipore). Subsequently, cells or sections were stained overnight with anti-ASC (1:200 or 1:500 AdipoGen AG-25B-0006, respectively) and anti-β III tubulin (1:1000, Abcam) antibodies. ASC and neuronal cells were visualized by using alexafluor 488- or 594-conjugated secondary antibodies (Thermo Fisher Scientific, 1:1000) and cell nuclei were visualized with DAPI (1:1000, Sigma Aldrich). Cover slips or sections were mounted on glass slides with FluorSave reagent (Merck Millipore).

Fluorescence and confocal microscopy

To assess ASC specks, pictures were taken with the confocal microscope STELLARIS 5 (Leica Microsystems), using three

laserlines: 405 nm, 590 nm and 499 nm. Emission windows were 425–504 nm for blue, 504–595 nm for green, and 595–750 nm for red. We used a pinhole of 1.0 Airy units at 580 nm (95.5 μm) and an objective of 63×/1.40 oil (NA 1.4, refractive index: 1.52). Confocal z-stacks (13–21 optical sections) were acquired with an optical section separation (z-interval) of 0.297 μm. Confocal z-stacks were used to create 3D rendered videos using the Leica Application Suite X (LAS X) software (Leica Microsystems).

Fluorescence images were acquired using the Olympus IX83 microscope (Olympus Life Science). We used a 40× (NA 0.75) dry objective. Pictures were analyzed with ImageJ 1.53c (NIH). To quantify ASC specks in culture, five pictures were acquired per well. The percentage of cells having at least one positive ASC speck was quantified in each picture and averaged over the four pictures per well. In DRG sections, ASC was quantified after imaging the entire DRG with the Olympus stage navigator function. The percentage of positive cells in each animal corresponds to the average of the three DRG collected for each animal.

Fluorescence-activated cell sorting (FACS) staining and data analysis

Lumbar DRG (L3–L5) were isolated and gently minced and digested at 37°C for 30 min with an enzyme cocktail containing 1 mg collagenase type I with 0.5 mg trypsin in 1 mL DMEM (Sigma-Aldrich) to obtain a single cell suspension. Cells were blocked using anti-Mo CD16/CD32 eBioscience™ (Invitrogen) and subsequently stained with a combination of fluorochrome-labeled antibodies (Table 2). Cells were stained for CD45 (immune cell marker), F4/80 (macrophage marker), Ly6G (neutrophil/granulocyte marker), and CD115 (monocytes). In addition, we used CD11b, Egr2, CD163, and CD206 and inducible nitric oxide synthase (iNOS) as markers for M1/M2 programming [26, 34]. Precision Count Beads™ (BioLegend) were added to each sample. Samples were filtered using pluriStrainer Mini 100 μm filters, before being transferred to tubes for measurement. Measurements were acquired using LSRFortessa flow cytometer (BD Biosciences) and analyzed with FACSDiva software. For all cellular analysis, we used the forward scatter and the side scatter (SSC) to identify events and live CD45⁺ singlets were manually gated for further analysis (Supplementary Fig. S3A). Experiments with males and females were performed in two different experimental cohorts.

Flow cytometry data were analyzed with OMIQ (Dotmatics, Inc., Boston, MA, <https://www.omiq.ai/>). Briefly, the raw FACS data containing the compensation matrix was imported to the OMIQ environment. Subsequently, the files were subsampled to include the same amount of events per file, the Uniform Manifold Approximation and Projection (UMAP) package was applied to the subsampled data to obtain a dimensional reduction map and FlowSOM was used to cluster the data.

Statistical analysis

Data presented as mean \pm SD or as mean \pm SEM. Data analyzed with GraphPad Prism version 9.3.0, using *t*-test (two-tailed, unpaired), one-way or two-way ANOVA, or two-way ANOVA with repeated measures, followed by post-hoc analysis. The details of all statistical tests and specific post-hoc analysis are indicated in the legend of each figure. A *P*-value less than 0.05 was considered statistically significant and each significance is indicated with **P* < 0.05, ***P* < 0.01, ****P* < 0.001.

Results

NLRP3 inflammasome activation in sensory neurons mediates the transition from acute to chronic inflammatory pain

To test whether NLRP3 inflammasome activation contributes to the transition from acute to chronic pain, we used a mouse model of hyperalgesic priming [35]. To that end, mice were injected intraplantar with carrageenan (1% w/v, 5 μ l) [16, 35]. Carrageenan induced a transient mechanical hypersensitivity that resolved within 3–4 days (Fig. 1A). At Day 7, intraplantar PGE₂ (100 ng/paw) induced mechanical hypersensitivity lasted 1 day in naive mice (non-primed). In contrast, PGE₂-induced mechanical hypersensitivity lasted at least 4 days in mice that had recovered from carrageenan-induced hyperalgesia (primed) (Fig. 1A), showing the presence of hyperalgesic priming after carrageenan. At Day 7, mRNA expression encoding for inflammasome-related genes *Nlrp3* and *Il18*, but not *Il1 β* , were significantly increased in lumbar DRG in primed mice compared to non-primed mice (Fig. 1B). To investigate if NLRP3 inflammasome was activated in sensory neurons *in vivo* after mice received the second inflammatory mediator PGE₂, to unmask the primed state, DRG were collected 6 h after intraplantar PGE₂ injection (100 ng/paw). At 6 h after PGE₂, the percentage of neurons with ASC specks, a measure of NLRP3 activation [19] was increased in primed mice compared to non-primed mice (Fig. 1C and D, Supplementary Videos S1 and S2).

To assess whether inflammatory mediators activate NLRP3 inflammasome *in vitro*, sensory neurons were stimulated with IL-1 β (50 ng/mL) and TNF (100 ng/mL), cytokines that are produced during carrageenan-induced inflammation [36]. Stimulation of sensory neurons with IL-1 β and TNF for 1 or 6 h significantly increased the percentage of neurons with ASC specks (Fig. 1E) and slightly increased the production of IL-18 at 6 h after stimulation but not at 1 h after stimulation (Supplementary Fig. S1B). Pre-treatment of sensory neurons with MCC950, a specific NLRP3 inflammasome inhibitor [37], prevented the cytokine-induced increase in ASC specks (Fig. 1E, Supplementary Fig. S1A). We previously identified that hyperalgesic priming induces an increase in mtROS

production in DRG neurons at Day 7 after carrageenan [16]. Considering that mtROS is one of the known triggers for NLRP3 inflammasome activation [18–20], we investigated the link between mtROS and NLRP3 inflammasome activity with our *in vitro* setup. To that end, sensory neurons were pre-treated for 1 h with mitoTEMPOL, a specific mtROS targeting antioxidant. Pre-treatment with mitoTEMPOL reduced the percentage of ASC⁺ neurons to a similar level as the vehicle condition (Fig. 1F), indicating that mtROS contributes to NLRP3 inflammasome activation induced by inflammatory mediators in sensory neurons.

Next, we tested the contribution of NLRP3 inflammasome activation to the prolongation of PGE₂-induced hyperalgesia after carrageenan priming. Carrageenan-primed and non-primed mice received a single intraperitoneal injection of MCC950 (10 mg/kg in saline solution) 15 min prior to intraplantar PGE₂. MCC950 did not affect the course of PGE₂-induced hyperalgesia in non-primed mice. In contrast, MCC950 pre-treatment prevented the persisting PGE₂-induced mechanical hyperalgesia in carrageenan-primed mice (Fig. 1G, Supplementary Fig. S1C). These data indicate that NLRP3 inflammasome activation contributes to the transition from acute to chronic inflammatory pain.

OA promotes oxidative stress and NLRP3 inflammasome activation in sensory neurons in a sex-dependent manner

Next, we investigated whether similar mechanisms are present in a rodent model of OA, where pain caused by joint damage transitions into a persisting pain [26, 38]. First, we investigated if changes in mitochondrial activity in sensory neurons occur during the course of monoiodoacetate-induced joint damage [16]. To that end, mice received an intra-articular injection of monoiodoacetate (MIA, 10% w/v, 10 μ l) in the ipsilateral knee and same volume of saline in the contralateral knee. In the first week, the MIA-induced OA model is characterized by joint inflammation, which disappears in the following weeks. In those weeks, the model is mainly characterized by joint damage and pain that is refractory to anti-inflammatory analgesics [27]. MIA induced mechanical hypersensitivity of the hind paw (Fig. 2A) and reduced weight bearing of the affected leg (Fig. 2B) in male and female mice starting from Day 3 until at least 21 days after MIA. At Day 7 or 21 after OA induction, the mitochondrial oxygen consumption rate (OCR) and the extracellular acidification rate (ECAR) of sensory neurons, as measures of mitochondrial respiration and anaerobic glycolysis, respectively, were statistically indistinguishable from baseline (Day 0). Similarly, we did not observe overt changes in the energetic profile of the sciatic nerves of mice with MIA-induced OA (Fig. 2C).

To assess mtROS production in sensory neurons during the course of OA, mice were injected intrathecal with MitoTracker™ Red CM-H2Xros, a dye that accumulates in mitochondria and fluoresces upon oxidation by mtROS [39]. At Day 7 after MIA injection, MitoTracker™ Red CM-H2Xros fluorescence in sensory neurons was decreased compared to Day 0. However, at Day 21 after MIA injection MitoTracker™ Red CM-H2Xros fluorescence was significantly elevated in sensory neurons of male and female mice (Fig. 2D, Supplementary Fig. S2A). Additionally, the number of MitoTracker™ Red CM-H2Xros positive neurons was significantly increased at Day 21 compared to Day 0 (Day 21:

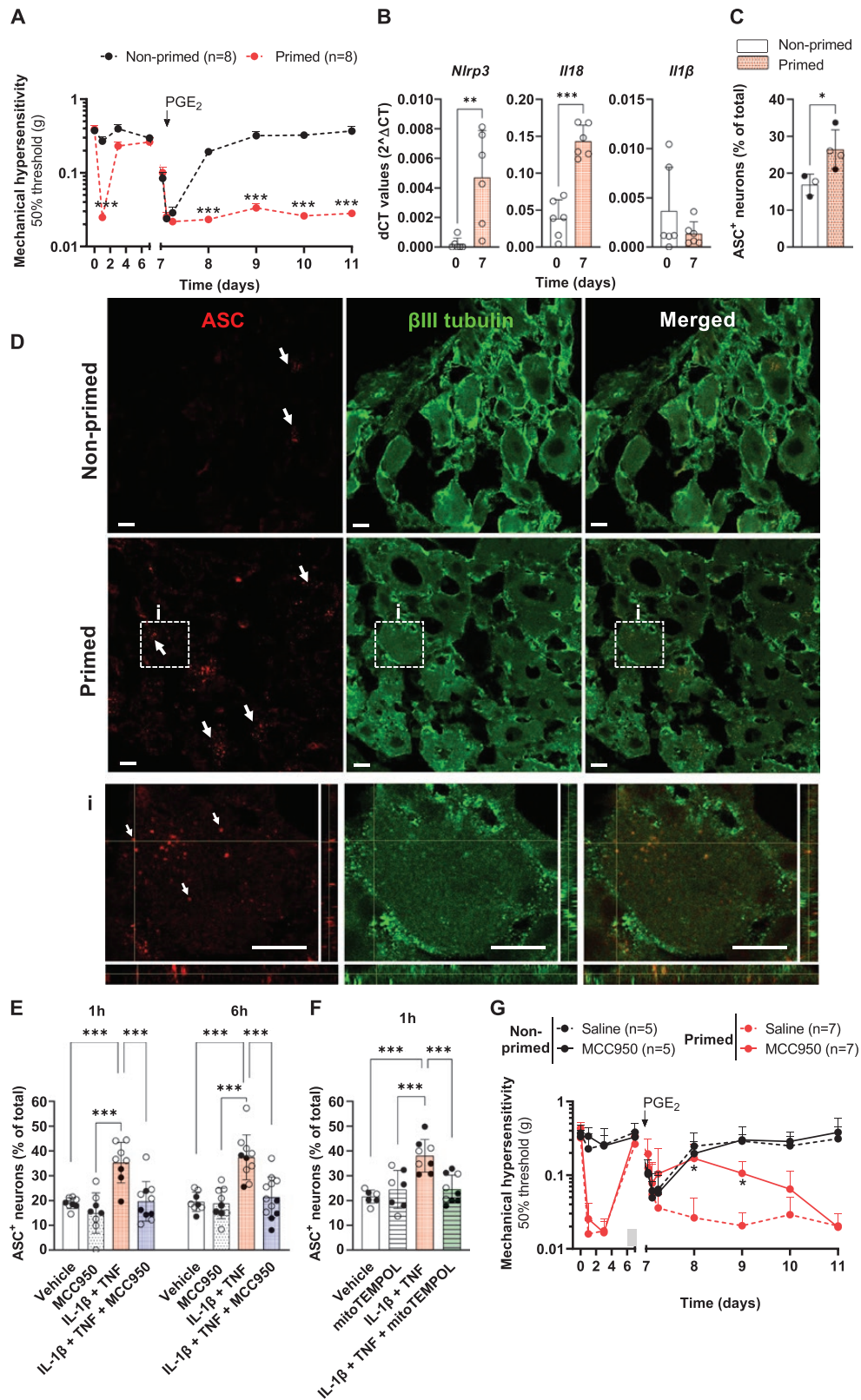


Figure 1. NLRP3 inflammasome activation promotes PGE₂-induced persistent hyperalgesia in primed mice. (A) Male and female mice were injected intraplantar with 1% (w/v) carrageenan or vehicle. At Day 7 after the initial injection, mice were injected intraplantar with 100 ng PGE₂. Course of mechanical hypersensitivity was followed over time with the von Frey test. Two-way repeated measures ANOVA with Sidak's post hoc. (B) At Day 7 after carrageenan or vehicle injection, expression of *Nlrp3*, *Il18*, and *Il1β* mRNA in the DRG was measured using RT-qPCR. Expression was corrected for expression of the housekeeping genes 18S, TBP, and Rictor. Unpaired two-tailed *t*-test. (C) At 6 h after intraplantar PGE₂, DRG were isolated and stained for ASC. The number of neurons with ASC specks in lumbar DRG were determined. Unpaired two-tailed *t*-test. (D) Representative pictures of the images of ASC specks and data shown in C. Scale bar = 20 μm. Examples of ASC specks are indicated by white arrows. (i) Orthogonal projections of selected area in representative picture of primed mice. The crosshair in the xy plane marks the spot shown in the xz (bottom) and yz

58/854 neurons *versus* naive: 7/1096 neurons, $P = 0.013$). The increase in MitoTracker™ Red CM-H2Xros fluorescence occurred predominantly in small diameter sensory neurons.

Next, we questioned if NLRP3 inflammasome activation is also present during the course of OA, where pain has become persistent. Expression of *Il18* mRNA was significantly increased at Day 3, while *Nlrp3* mRNA was increased at Day 21 after MIA compared to Day 0 in male mice. In female mice, *Il18* and *Nlrp3* mRNA expression were unaffected (Fig. 2E). The expression of *Il1 β* and *Il6* (general inflammation marker) mRNA was not significantly different during the course of OA in male or female mice (Fig. 2E). To assess whether NLRP3 activation occurred within neurons, DRG from mice with MIA-induced OA were stained for ASC. The number of neurons with ASC specks in the ipsilateral DRG was ~4-fold higher at Day 21 after MIA compared to naive mice or compared to the contralateral DRG. The number of ASC specks in the contralateral DRG did not differ from DRG of naive mice (Fig. 2F and G; Supplementary Videos S3 and S4). The percentage of ASC⁺ neurons at the ipsilateral DRG was significantly higher in males than females at 21 days after OA induction (Fig. 2F).

NLRP3 inflammasome activation contributes to OA pain

Next, we assessed whether inhibition of the NLRP3 inflammasome contributes to pain in OA, by either inhibiting NLRP3 inflammasome assembly during early or established MIA-induced OA. To inhibit NLRP3 inflammasome activation after initial OA development, mice received daily intraperitoneal MCC950 (10 mg/kg) injections from Days 7 to 9. We selected Day 7 as starting point for MCC950 treatment, because previous data indicate that after Day 7 pain becomes independent of the original damage in this model [26]. MCC950 transiently reduced MIA-induced mechanical hypersensitivity in male and female mice (Fig. 3A and B). However, MCC950 did not affect MIA-induced deficits in weight bearing (Fig. 3C). Strikingly, when MCC950 was injected from Days 21 to 23 during established OA, the treatment reversed mechanical hyperalgesia in males for at least one week (Fig. 3A). In females, the same treatment regimen reduced mechanical hypersensitivity for only 3 days (Fig. 3B). MCC950 treatment during established OA normalized MIA-induced deficits in weight bearing in males and females at 24 h after the last MCC950 injection (Fig. 3D). At Day 28, one week after the last MCC950 injection, the percentage of DRG neurons with ASC specks was significantly decreased in males with MIA-induced OA, but not in females (Fig. 3E), which may explain why the analgesic effect was more prolonged in males. Because intraperitoneal administration of

MCC950 may affect NLRP3 inflammasome activation not only in the DRG, but also other tissues, such as the joint, we tested whether intrathecal administration of the NLRP3 inflammasome inhibitor also attenuated pain in established OA. Daily intrathecal injections of MCC950 (5 μ M), from Days 21 to 23, significantly reversed mechanical hypersensitivity (Fig. 3F) and weight bearing deficits (Fig. 3G) in male and female mice with MIA-induced OA. Overall, these data suggest that NLRP3 inflammasome activation in DRG neurons maintains OA pain in a sex-dependent manner.

Effect of NLRP3 inflammasome inhibition in DRG immune composition during chronic OA

DRG infiltrating macrophages with a pro-inflammatory M1-like phenotype are important to maintain OA pain [26]. NLRP3 inflammasome activation ultimately results in the production of pro-inflammatory cytokines IL-18 and IL-1 β , which may promote immune cell accumulation or programming of DRG macrophages into an inflammatory M1-like phenotype [40]. Thus, we questioned whether the DRG immune cell populations were affected by NLRP3 inflammasome inhibition. Immune cells composition was assessed by flow cytometry, using the gating strategy depicted in Supplementary Fig. S3A. To assess the potential effect of NLRP3 inflammasome inhibition on immune cell populations, a dimensional reduction analysis was performed using UMAP, followed by clustering analysis with FlowSOM to identify immune cell clusters (Fig. 4A). The number of cells in each cluster did not differ between control-treated and MCC950-treated mice, indicating that the overall immune cells population numbers were not affected (Fig. 4B). However, when we assessed male and females separately, of all six identified clusters, the percentage of cells represented by cluster 5 (containing CD11b^{high}F4/80^{dim} Ly6G^{low} cells) was reduced after MCC950 treatment in males (Fig. 4C). In females, we did not observe differences.

Next, we assessed whether expression of any specific marker for M1/M2 programming were affected in populations expressing macrophage associated markers F4/80 and CD11b (clusters 3, 4, 5, and 6). Interestingly, the expression of pro-algesic and pro-inflammatory M1-like marker iNOS [26, 34] was reduced in cluster 5 after MCC950 treatment in males, but not in females (Fig. 4D). The expression of iNOS, CD206 or Egr2 were not affected by MCC950 treatment in any other clusters (Supplementary Fig. S3B).

Discussion

In this study, we investigated the role of mitochondria and NLRP3 inflammasome activation in the transition from acute

(side) projections. Scale bar = 5 μ m. Examples of ASC specks are indicated by white arrows. (E) Sensory neurons were stimulated with IL-1 β (50 ng/mL) + TNF (100 ng/mL). To block NLRP3 inflammasome activation, MCC950 (1 μ M) was added to the medium 1 h prior to the addition of cytokines. After 1 h or 6 h, cells were fixed and stained for ASC and β III tubulin. A neuron was counted as positive if at least one ASC speck was present. One-way ANOVA with Dunnett's multiple comparison test. (F) Sensory neurons were stimulated with IL-1 β (50 ng/mL) + TNF (100 ng/mL). To prevent the formation of mitochondrial ROS, mitoTEMPOL (500 nM) was added to the medium 1 h prior to the addition of cytokines. After 1 h, cells were fixed and stained for ASC and β III tubulin. A neuron was counted as positive if at least one ASC speck was present. One-way ANOVA with Dunnett's multiple comparison test. (G) Mice (males and females) were injected intraplantar with 1% (w/v) carrageenan. At Day 7 after the initial injection, mice were injected intraplantar with 100 ng PGE₂. Mice received a single intraperitoneal injection of MCC950 (10 mg/kg) or vehicle 15 min prior to intraplantar PGE₂ injection (indicated by gray box). Course of mechanical hypersensitivity followed over time using the von Frey test, in carrageenan- or non-primed male and female mice. Two-way repeated-measures ANOVA with Sidak's post hoc. Open circles correspond to females, closed circles to male. Data are represented as mean \pm SD, * P < 0.05; ** P < 0.01; *** P < 0.001.

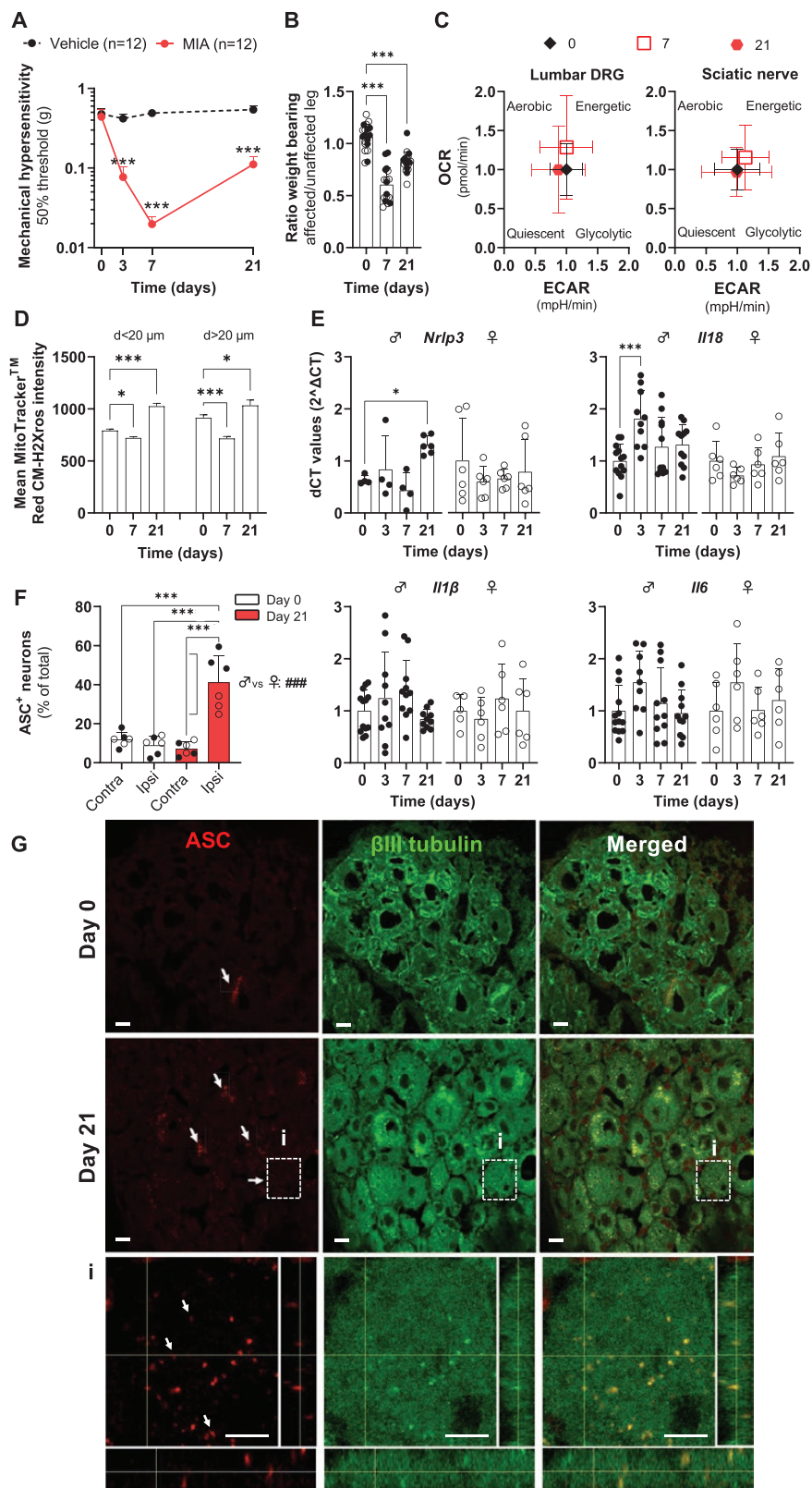


Figure 2. mtROS and NLRP3 inflammasome activation in DRG neurons during OA. Mice (males and females) received an intra-articular injection of MIA (10 μl , 10%) in one knee and the same volume of saline on the other knee. (A) Course of mechanical hyperalgesia was followed over time using von Frey test, two-way ANOVA followed by Sidak's multiple comparison test, or (B) dynamic weight bearing to assess postural deficits. One-way ANOVA followed by Dunnett's multiple comparison tests. (C) Basal oxygen consumption rate (OCR) and extracellular acidification rates (ECAR) were measured in DRG neurons and sciatic nerves isolated from mice (males and females) at the indicated time points after MIA. Data are expressed relative to Day 0. One-way ANOVA followed by Dunnett's multiple comparison tests. $n = 9, 11, 10$ for days 0, 7, 21, respectively; for sciatic nerves, $n = 12, 15, 14$ for days 0, 7, 21, respectively. (D) MitoTracker™ Red CM-H2Xros (100 μM) was injected 6h prior to isolation of DRG to visualize mtROS production. Mean MitoTracker™ Red CM-H2Xros intensity was measured in small ($d < 20 \mu\text{m}$) and medium/large-diameter (d) neurons (>20 μm) at indicated days after

to persistent inflammation-induced nociceptive pain and in MIA-induced inflammatory OA pain. We detected that mtROS production and NLRP3 activation in DRG neurons were increased in a hyperalgesic priming model, where acute inflammatory pain transitions into a persisting one. In mice with established OA pain, sensory neurons also produced more mtROS, but without overt changes in mitochondrial respiration. Importantly, blocking the NLRP3 inflammasome pathway prevented the transition to persistent inflammatory pain and attenuated OA pain. Overall, these data indicate that NLRP3 inflammasome activation in sensory neurons, potentially caused by neuronal mitochondrial-derived oxidative stress, promotes the transition to chronic pain.

We identified that inflammasome activation contributes to pain in two different models: hyperalgesic priming and OA. Hyperalgesic priming models the transition from acute to persistent inflammation-induced nociceptive pain, caused by changes in sensory neurons that linger beyond the resolution of the initial inflammation. Thus, our data indicate that NLRP3 inflammasome activation may be critical for the transition to persistent inflammatory pain. To what extent a similar transition from acute to persistent pain occurs in the OA model is unclear. Importantly, in the OA model used, pain persists independently of the degree damage/inflammation [26], suggesting it may have transitioned to a more persisting state in which local changes at the joint level do not determine pain intensity. For example, depletion of nervous tissue macrophages is sufficient to attenuate pain [26]. The question arises whether the initial damage or inflammation in OA triggers similar mechanisms as in the hyperalgesic priming model? Evidence suggests that intermittent pain flares in OA become longer, more frequent and intense as the disease progresses, eventually leading to constant pain and joint failure [38]. Moreover, initial damage in the joint may prime the nervous system, as well as trigger the subsequent release of inflammatory mediators like PGE₂, which is known to be one of the main catabolic factors involved in OA [41, 42]. Thus, repeated triggers that initially lead to acute pain, ultimately may result in the transition to chronic pain through activation of the NLRP3 inflammasome pathway.

We identified that sensory neurons produced more mtROS after the induction of OA or after hyperalgesic priming, but we do not know the upstream triggers of this increase. A possible cause for increased mtROS is elevated mitochondrial respiration [16]. Indeed, in the hyperalgesic priming model, mitochondrial respiration was enhanced in sensory neurons [16]. However, mitochondrial respiration was not affected in sensory neurons during OA. This indicates that either model-specific differences exist in the upstream mechanisms leading to the neuronal oxidative stress or that changes in mitochondrial respiration do not drive the increase in mtROS

production. Inflammatory cytokines and damage-associated molecular patterns in joint tissue promote neuronal firing [43, 44], which increases mitochondrial Ca²⁺ levels [45] and can trigger mtROS production [46]. Indeed, inflammatory cytokines promote ROS production in neurons [47, 48]. Conversely, some evidence exists that inflammasome activation may cause mitochondrial dysfunction [49], further promoting mtROS production. Another difference between the models is the duration of pain reduction after systemic MCC950 administration. Importantly, mice with hyperalgesic priming received only one injection, while MIA mice received three injections. MCC950, a reversible NLRP3 inflammasome inhibitor, has a half-life of only 3.27 hours [37], so our data suggest that more injections or a higher dose may be required to permanently block inflammasome activation. Another possibility is that ongoing mitochondrial dysfunction (increased mtROS production), which is upstream of inflammasome activation, is not blocked by MCC950 administration, therefore it continues to drive inflammasome activation after a transient block. Recent work indeed suggests that an increase in the mitochondrial protein ATP5c-KMT may cause ongoing elevated superoxide production and contributes to hyperalgesic priming [15, 16].

Inflammasome activation is classically associated with immune cell activation. In our study, most ASC specks were found in sensory neurons. We detected NLRP3 inflammasome activation in mouse DRG neurons in models of hyperalgesic priming and OA. We have not investigated whether NLRP3 inflammasome activation occurs in other cells in the DRG, such as immune cells. Thus, we cannot exclude that NLRP3 inflammasome activation in non-neuronal DRG cells may occur and contribute to pain. Interestingly, signs of NLRP3 inflammasome activation have been observed in cortical neurons in the context of migraine [50], as well as in spinal cord neurons, glia and astrocytes in models of cancer-induced bone pain and neuropathic pain [51–56]. Moreover, pharmacological or genetic inhibition of the NLRP3 inflammasome reduces inflammation-, surgery-, bone cancer-, chemotherapy-, and nerve injury-induced pain [51, 54, 57, 58] and spinal IL-1 β and IL-18 release [55, 59, 60]. Intriguingly, studies have shown that all these models are associated with mitochondrial dysfunction and oxidative stress, further supporting a role of oxidative stress in activation of the NLRP3 inflammasome pathway. Additionally, recent single-nucleus RNA-seq data shows *NLRP3*, *PYCARD* (ASC gene), *CASP1*, and *IL18* expression in several human DRG neurons subtypes [61], indicating sensory neurons have the relevant machinery for NLRP3 inflammasome activation. Importantly, *NLRP3* expression is increased in DRG of patients with neuropathic pain compared to patients without pain [62]. Thus, NLRP3 inflammasome activation appears to be a common

MIA injection in male and female mice. Small-diameter $n = 622$ – 1045 cells, medium/large-sized = 232 – 402 cells from four mice per group. One-way ANOVA followed by Dunnett's multiple comparison tests. (E) Expression of *Nlrp3*, *Il18*, *Il1 β* , and *Il6* mRNA in the DRG at Days 0, 3, 7, and 21 after MIA injection. Data were normalized for housekeeping genes 18S and B2M and expressed relative to Day 0. One-way ANOVA followed by Dunnett's multiple comparison tests. (F) Immunofluorescent staining of ASC specks at Day 0 and Day 21. A neuron was considered positive for ASC if at least one ASC speck was visible in the soma. One-way ANOVA followed by Dunnett's multiple comparison tests. (G) Representative pictures of the images of ASC specks and data shown in F (ipsilateral side). Scale bar = $20\ \mu\text{m}$. Examples of ASC specks are indicated by white arrows. (i) Orthogonal projections of selected area in representative picture of Day 21 after MIA. The crosshair in the xy plane marks the spot shown in the xz (bottom) and yz (side) projections. Scale bar = $5\ \mu\text{m}$. Examples of ASC specks are indicated by white arrows. Open circles correspond to females and closed circles to males. Data represented as mean \pm SD, except in graph D where data is visualized as mean \pm SEM. * $P < 0.05$; ** $P < 0.01$; *** $P < 0.001$.

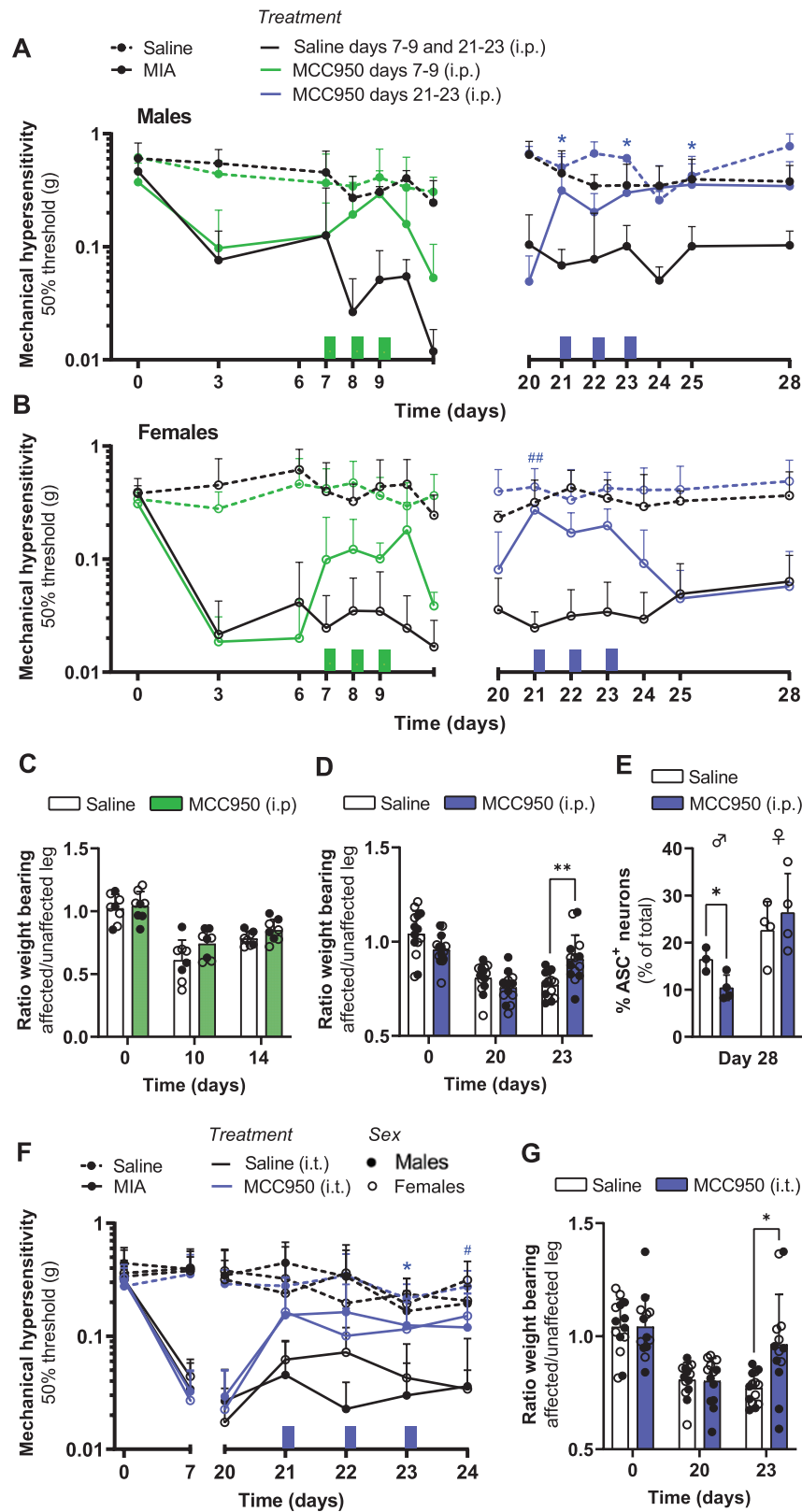


Figure 3. Inhibition of NLRP3 inflammasome activation attenuates OA pain. Mice received an intra-articular injection of MIA (10 μ l, 10%) in one knee joint and saline in the contralateral knee. From Day 7 to 9 or from 21 to 23, mice received intraperitoneal injections of MCC950 (10 mg/kg) daily (time of injections are represented by rectangular boxes above the x axis). The control group received saline at all timepoints (7–9 and 21–23). Course of mechanical sensitivity was followed over time with von Frey ($n = 4$ per group) in (A) male mice or (B) female mice. * $P < 0.05$ saline versus MCC950 in males with MIA-induced OA. # $P < 0.05$ saline vs. MCC950 in females mice with MIA-induced OA. Two-way repeated-measures ANOVA with Sidak's post hoc multiple comparison test. (C–D) Course of changes in weight distribution of hind legs measured using dynamic weight bearing in mice that received MCC950 from (C) Day 7 to 9 or (D) Day 21 to 23. Two-way repeated-measures ANOVA with Sidak's post hoc multiple comparison test. (E) At Day 28 after MIA injection, DRG were stained for ASC and the number of ASC⁺ DRG neurons was determined. Unpaired two-tailed t test. (F) Mice were

mechanism that occurs in various pain types, when mitochondrial dysfunction is present, and may actively contribute to pain.

How does NLRP3 inflammasome activation occur in neurons? Classically, NLRP3 inflammasome activation has been described as a two-step process [18–20]. Activation of cytokine receptors (e.g. IL-1 receptor and TNF receptor) promotes NLRP3 and pro-IL-1 β expression, so is an example of a first priming step [56]. IL-1 β and TNF were used to stimulate neurons *in vitro*, because these cytokines are produced during carrageenan-induced inflammation and play a role in the development of OA [36, 63]. For example, TNF and IL-1 β are significantly increased in the joints of osteoarthritis patients, in comparison to healthy controls [64]. *In vitro*, we found that stimulation of sensory neurons with IL-1 β and TNF was sufficient to stimulate ASC speck formation, which indicates NLRP3 inflammasome activation occurred, leading us to question if a two-step activation is required in neuronal cells. The axotomy performed to obtain sensory neurons for culture may correspond to the priming step, while stimulation with cytokines is the activation step. Indeed, sciatic nerve axotomy promotes *Nlrp3*, *Casp1*, and *Il1b* expression in spinal cord motoneurons [65]. Stimulation with inflammatory cytokines may also promote mtROS production, which could trigger the inflammasome activation step. Indeed, pre-treatment of sensory neurons with a mitochondria targeting antioxidant decreased ASC speck formation, a sign of NLRP3 inflammasome activation, in sensory neurons stimulated with inflammatory cytokines. *In vivo*, a transient local inflammation increased expression of NLRP3 inflammasome components and promoted mitochondrial dysfunction in sensory neurons (priming step), and subsequent intraplantar PGE₂ injection induced NLRP3 inflammasome activation [43, 44, 66]. Indeed, evidence exists that PGE₂ can activate the NOX2-ROS-NLRP3 inflammasome axis in hematopoietic stem cells [67]. Future work should elucidate how exactly PGE₂ induces NLRP3 inflammasome activation in neurons.

An important question is how inflammasome activation may contribute to pain and altered neuronal excitability. NLRP3 inflammasome activation is required for the release of pro-inflammatory cytokines (IL-1 β and IL-18), which activate sensory neurons directly [22], but also may activate local satellite glial cells [23, 24, 68], or program nervous tissue macrophages into a pro-inflammatory M1-like state. M1-like macrophages are required in the DRG to maintain OA pain [26]. We observed that inflammasome inhibition induced a modest decrease in the number of F4/80^{dim}- CD11b⁺-Ly6G^{low} cells. Moreover, iNOS expression was reduced in this population in males after MCC950 treatment. These data suggest that inflammasome activation may contribute, in combination with other potential non-inflammasome related processes (Martin Gil *et al.*, submitted), to the pro-inflammatory programming of macrophages in OA.

Intra-articular injection of MIA disrupts chondrocyte glycolysis and results in chondrocyte death, bone necrosis and

inflammation [27]. Given the local respiratory effects in the joint and its neurotoxicity [69], MIA could also directly affect energy production in the sensory neurons. Nonetheless, we did not observe any overt changes in the energetic profile of DRG neurons in mice shortly after they received an intra-articular injection of MIA. In addition, MIA could induce NLRP3 inflammasome activation in the joint. Thus, it is possible that the systemically administered NLRP3 inflammasome inhibitor MCC950 also reduced pain through improvements in the joint pathology. Indeed, some evidence exists that NLRP3 inflammasome activation in the joint contributes to pain and loss of articular cartilage in a rat destabilization of the medial meniscus OA model [70]. Nevertheless, we showed that intrathecal injection of the NLRP3 inflammasome inhibitor, which only targets DRG/spinal cord, reduced pain-associated behaviors at least to the same extent as systemic administration, indicating that inhibition of the NLRP3 inflammasome in the DRG/spinal cord is sufficient to reduce OA pain. Strikingly, NLRP3 inflammasome inhibition reduced mechanical hypersensitivity longer in males than in females, suggesting sex differences in the contribution of NLRP3 inflammasome to MIA-induced OA pain. Moreover, NLRP3 inflammasome inhibition reduced iNOS expression in the cluster F4/80^{dim}- CD11b⁺-Ly6G^{low} in males only. Sex-specific contribution of inflammasome activation is also found in other pain models. NLRP3 deficiency reduces post-operative pain in males, whilst in females NLRP3 deficiency had less impact on post-operative pain [58]. Similarly, in COVID, abdominal aortic aneurysm, and myocarditis, male patients have more pronounced NLRP3 inflammasome activation than females [71–73]. Some suggestions point towards testosterone promoting NLRP3 inflammasome activation, while estrogen inhibits this pathway [73]. Thus, our findings add to the growing evidence of sex-specific mechanisms that contribute to pain [74–81]. For example, there is some sexual dimorphism in the distribution of DRG infiltrating macrophages in the context of complete Freund's adjuvant-induced inflammatory pain and nerve injury-induced pain, although these differences did not directly affect the pain phenotype [81, 82]. Furthermore, spinal activation of toll-like receptor 4 (TLR4) and spinal microglia contribute to mechanical hypersensitivity in spared nerve injury induced-neuropathic pain in males only [75, 79]. Sex differences may also affect analgesic treatment, as we show a sex-specific effect of MCC950. Similarly, evidence exists that women require higher morphine concentrations to achieve similar pain relief as men [83, 84]. Thus, both sexes should be studied when exploring new targets for pain treatment.

In conclusion, NLRP3 inflammasome activation in DRG neurons contributes to chronic pain development. We identified that neuronal NLRP3 inflammasome activation contributes to OA pain in a sex-dependent manner. Blocking NLRP3 inflammasome may therefore be a potential therapeutic strategy to treat chronic OA pain. Some preliminary clinical evidence shows that compounds targeting the NLRP3 inflammasome (dapansutrile) or its downstream products (anakinra and canakinumab) reduced pain in small cohorts of

injected intra-articularly with MIA (10 μ l, 10%). From Day 21 to 23 (blue boxes), mice were injected intrathecally with MCC950 (5 μ l, 5 μ M) daily. Course of mechanical hypersensitivity was assessed using von Frey ($n = 7$ per group). * $P < 0.05$ saline versus MCC950 in males with MIA-induced OA. # $P < 0.05$ saline vs. MCC950 in female mice with MIA-induced OA. Two-way repeated-measures ANOVA with Sidak's post hoc multiple comparison test. (G) Course of changes in weight distribution of hind legs measured using dynamic weight bearing in mice that received MCC950 from Day 21 to 23. Two-way repeated-measures ANOVA with Sidak's post hoc multiple comparison test. Open circles correspond to females, closed circles to males. Data are represented as mean \pm SD. * $P < 0.05$; ** $P < 0.01$. Green and blue colour coding has been used to indicate NLRP3 treatment at Days 7–9 or Days 21–23 respectively. For colour figure refer online version.

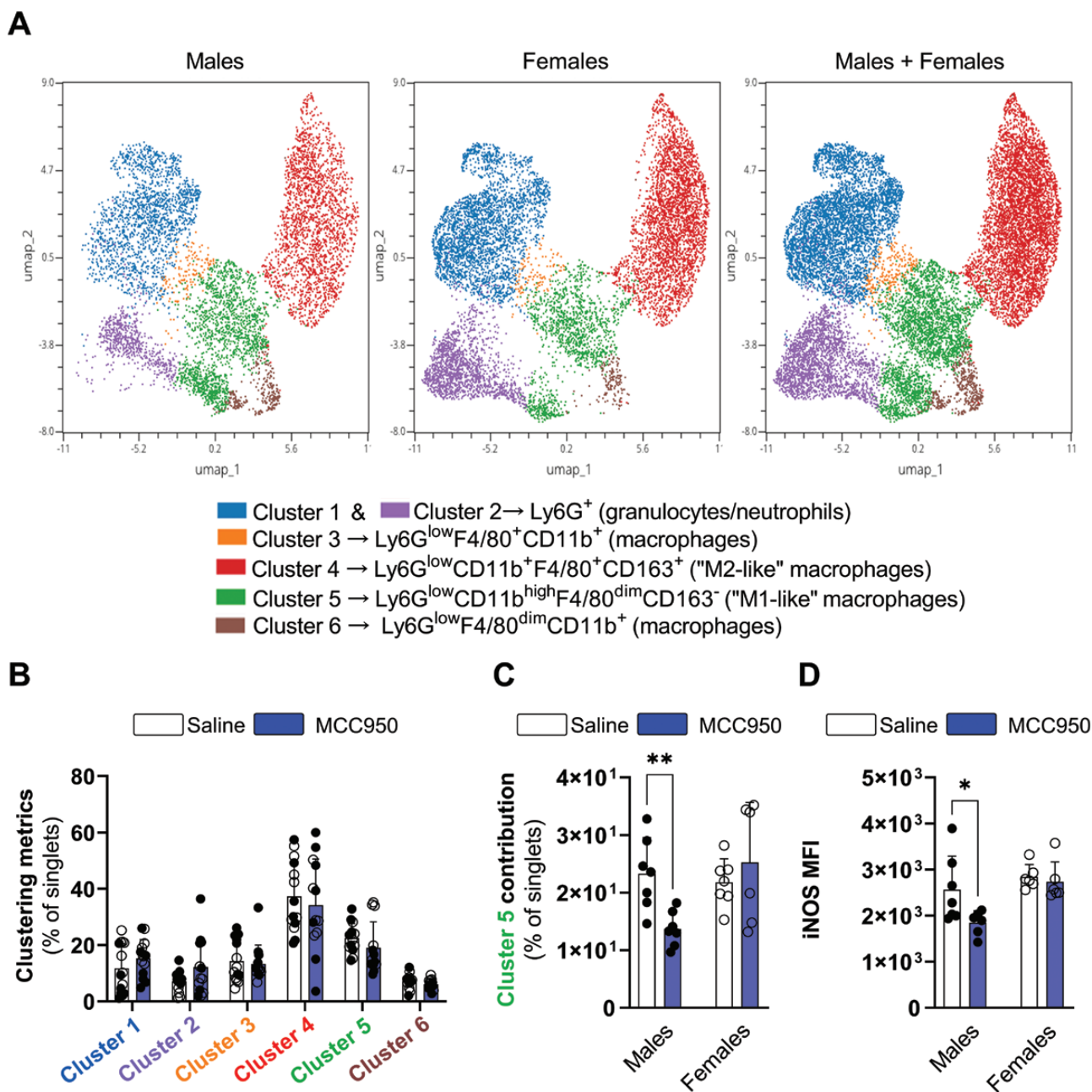


Figure 4. Effect of NLRP3 inflammasome inhibition in DRG immune composition during chronic OA. MIA (10 μ l, 10%) was injected intra-articularly in the ipsilateral knee. Saline was injected in the contralateral knee. From Days 21 to 23 mice received an intrathecal injection of MCC950 (5 μ l, 5 μ M) to inhibit NLRP3 inflammasome. DRG were isolated at Day 24 after MIA injection and processed for FACS analysis. FlowSOM analysis was applied to the population identified as live CD45⁺ single cells. (A) UMAP projection of the FACS dataset with cluster results obtained with FlowSOM overlaid. (B) Cluster contribution of the clusters identified using FlowSOM. (C) Representation of cluster 5 contribution in males or females after saline or MCC950 treatment. Unpaired two-tailed *t* test. (D) Mean fluorescence intensity (MFI) of iNOS in cluster 5. Unpaired two-tailed *t* test. Open circles correspond to females, closed circles to males. Data represented as mean \pm SD. **P* < 0.05; ***P* < 0.01.

patients with gout flare [85], juvenile idiopathic arthritis, and Schnitzler syndrome [86, 87]. Larger clinical studies should assess efficacy of inhibiting NLRP3 inflammasome to treat OA pain in male and female patients.

Supplementary material

Supplementary data are available at *Immunotherapy Advances* online.

Acknowledgments

We would like to thank Maura Bom for the help with the analysis of immunofluorescence pictures, Lucie Groenendaal and Marleen Meliefste for the help with the analysis of dynamic weight bearing data. Graphical abstract was created with BioRender.com. The Editor-in-Chief, Tim Elliott, and handling editor, Menno van Zelm, would like to thank the following reviewers, Shafaq Sikandar and an anonymous reviewer, for their contribution to the publication of this article.

Author contributions

P.S.S.R. – conceptualization, investigation, formal analysis, visualization, writing; S.V. – investigation; C.M.G. – investigation. H.L.D.M.W. – supervision, reviewing, and editing; N.E. – funding, conceptualization, visualization, supervision, reviewing, and editing.

Funding

This work has been supported by European Union's Horizon 2020 research and innovation program under the Marie Skłodowska-Curie grant agreement No 814244. H.L.D.M.W. is funded by the Netherlands Organization for Scientific Research (NWO), under the grant 016.VENI.192.053.

Conflict of interest

None declared.

Ethics approval

The animal research adhered to the ARRIVE guidelines (<https://arriveguidelines.org/arrive-guidelines>).

Data availability

Data are available in the manuscript or as supplemental information. Raw data are available on request.

References

- Schild M, Müller U, von Schenck U *et al.* The burden of chronic pain for patients with osteoarthritis in Germany: a retrospective cohort study of claims data. *BMC Musculoskelet Disord* 2021; 22(1):317. <https://doi.org/10.1186/s12891-021-04180-1>
- Szekanecz Z, McInnes IB, Schett G *et al.* Autoinflammation and autoimmunity across rheumatic and musculoskeletal diseases. *Nat Rev Rheumatol* 2021; 17(10):585–95. <https://doi.org/10.1038/s41584-021-00652-9>
- Wylde V, Beswick A, Bruce J *et al.* Chronic pain after total knee arthroplasty. *EFORT open Rev* 2018; 3(8):461–70. <https://doi.org/10.1302/2058-5241.3.180004>
- Taylor P, Manger B, Alvaro-Gracia J *et al.* Patient perceptions concerning pain management in the treatment of rheumatoid arthritis. *J Int Med Res* 2010; 38(4):1213–24. <https://doi.org/10.1177/147323001003800402>
- Lee YC, Frits ML, Iannaccone CK *et al.* Subgrouping of patients with rheumatoid arthritis based on pain, fatigue, inflammation, and psychosocial factors. *Arthritis Rheumatol (Hoboken, N.J.)* 2014; 66(8):2006–14. <https://doi.org/10.1002/art.38682>
- Urits I, Gress K, Charipova K *et al.* Use of cannabidiol (CBD) for the treatment of chronic pain. *Best Pract Res Clin Anaesthesiol* 2020; 34(3):463–77. <https://doi.org/10.1016/j.bpa.2020.06.004>
- Rangaraju V, Lewis TL, Hirabayashi Y *et al.* Pleiotropic mitochondria: the influence of mitochondria on neuronal development and disease. *J Neurosci* 2019;39(42):8200–8. <https://doi.org/10.1523/JNEUROSCI.1157-19.2019>
- Lagos-Rodríguez V, Martínez-Palma L, Marton S *et al.* Mitochondrial bioenergetics, glial reactivity, and pain-related behavior can be restored by dichloroacetate treatment in rodent pain models. *Pain* 2020; 161(12):2786–97. <https://doi.org/10.1097/j.pain.0000000000001992>
- Peters MJ, Broer L, Willems HLDM *et al.* Genome-wide association study meta-analysis of chronic widespread pain: evidence for involvement of the 5p152 region. *Ann Rheum Dis* 2013; 72(3):427–36. <https://doi.org/10.1136/annrheumdis-2012-201742>
- Park ES, Gao X, Chung JM *et al.* Levels of mitochondrial reactive oxygen species increase in rat neuropathic spinal dorsal horn neurons. *Neurosci Lett* 2006; 391(3):108–11. <https://doi.org/10.1016/j.neulet.2005.08.055>
- Shin HJ, Park H, Shin N *et al.* Pink1-mediated chondrocytic mitophagy contributes to cartilage degeneration in osteoarthritis. *J Clin Med* 2019; 8(11):1849. <https://doi.org/10.3390/jcm8111849>
- Meng W, Hao M-M, Yu N *et al.* 2-Bromopalmitate attenuates bone cancer pain via reversing mitochondrial fusion and fission imbalance in spinal astrocytes. *Mol Pain* 2019; 15(1):1744806919871813. <https://doi.org/10.1177/1744806919871813>
- Flatters SJL. The contribution of mitochondria to sensory processing and pain. *Prog Mol Biol Transl Sci* 2015; 131:119–46. <https://doi.org/10.1016/bs.pmbts.2014.12.004>
- Bittar A, Jun J, La JH *et al.* Reactive oxygen species affect spinal cell type-specific synaptic plasticity in a model of neuropathic pain. *Pain* 2017; 158(11):2137–46. <https://doi.org/10.1097/j.pain.0000000000001014>
- Willems HLDM, Kavelaars A, Prado J *et al.* Identification of FAM173B as a protein methyltransferase promoting chronic pain. *PLoS Biol* 2018; 16(2):e2003452. <https://doi.org/10.1371/journal.pbio.2003452>
- Willems HLDM, Silva Santos Ribeiro P, Broeks M *et al.* Inflammation-induced mitochondrial and metabolic disturbances in sensory neurons control the switch from acute to chronic pain. *bioRxiv* 2022. [Preprint]. <https://doi.org/10.1101/2022.08.29.505682>
- Marouf BH, Hussain SA, Ali ZS *et al.* Resveratrol supplementation reduces pain and inflammation in knee osteoarthritis patients treated with meloxicam: a randomized placebo-controlled study. *J Med Food* 2018; 21(12):1253–9. <https://doi.org/10.1089/jmf.2017.4176>
- Huang Y, Xu W, Zhou R. NLRP3 inflammasome activation and cell death. *Cell Mol Immunol* 2021; 18(9):2114–27. <https://doi.org/10.1038/s41423-021-00740-6>
- Kelley N, Jeltama D, Duan Y *et al.* The NLRP3 inflammasome: an overview of mechanisms of activation and regulation. *Int J Mol Sci* 2019; 20(13):3328. <https://doi.org/10.3390/ijms20133328>
- Milner MT, Maddugoda M, Götz J *et al.* The NLRP3 inflammasome triggers sterile neuroinflammation and Alzheimer's disease. *Curr Opin Immunol* 2021; 68:116–24. <https://doi.org/10.1016/j.coi.2020.10.011>
- Binshtok AM, Wang H, Zimmermann K *et al.* Nociceptors are interleukin-1beta sensors. *J Neurosci Off J Soc Neurosci* 2008; 28(52):14062–73. <https://doi.org/10.1523/JNEUROSCI.3795-08.2008>
- Pilat D, Piotrowska A, Rojewska E *et al.* Blockade of IL-18 signaling diminished neuropathic pain and enhanced the efficacy of morphine and buprenorphine. *Mol Cell Neurosci* 2016; 71:114–24. <https://doi.org/10.1016/j.mcn.2015.12.013>
- Miyoshi K, Obata K, Kondo T *et al.* Interleukin-18-mediated microglia/astrocyte interaction in the spinal cord enhances neuropathic pain processing after nerve injury. *J Neurosci Off J Soc Neurosci* 2008; 28(48):12775–87. <https://doi.org/10.1523/JNEUROSCI.3512-08.2008>
- Liu S, Liu Y-P, Lv Y *et al.* IL-18 contributes to bone cancer pain by regulating glia cells and neuron interaction. *J Pain* 2018; 19(2):186–95. <https://doi.org/10.1016/j.jpain.2017.10.003>
- Faul F, Erdfelder E, Buchner A *et al.* Statistical power analyses using G*Power 31: tests for correlation and regression analyses. *Behav Res Methods* 2009; 41(4):1149–60. <https://doi.org/10.3758/BRM.41.4.1149>
- Raouf R, Martin Gil C, Lafeber FPJG *et al.* Dorsal root ganglia macrophages maintain osteoarthritis pain. *J Neurosci* 2021; 41(39):8249–61. <https://doi.org/10.1523/JNEUROSCI.1787-20.2021>

27. Pitcher T, Sousa-Valente J, Malcangio M. The monoiodoacetate model of osteoarthritis pain in the mouse. *J Vis Exp* 2016; 16(111):53746. <https://doi.org/10.3791/53746>
28. Stokes JA, Corr M, Yaksh TL. Transient tactile allodynia following intrathecal puncture in mouse: contributions of Toll-like receptor signaling. *Neurosci Lett* 2011; 504(3):215–8. <https://doi.org/10.1016/j.neulet.2011.09.025>
29. van Eenige R, Verhave PS, Koemans PJ et al. RandoMice, a novel, user-friendly randomization tool in animal research. *PLoS One* 2020; 15(8):e0237096. <https://doi.org/10.1371/journal.pone.0237096>
30. Chaplan SR, Bach FW, Pogrel JW et al. Quantitative assessment of tactile allodynia in the rat paw. *J Neurosci Methods* 1994; 53(1):55–63. [https://doi.org/10.1016/0165-0270\(94\)90144-9](https://doi.org/10.1016/0165-0270(94)90144-9)
31. Prado J, Popov-Celeketic J, Steen-Louws C et al. Development of recombinant proteins to treat chronic pain. *JoVE* 2018; 11(134):e57071. <https://doi.org/10.3791/57071>
32. Krukowski K, Ma J, Golonzhka O et al. HDAC6 inhibition effectively reverses chemotherapy-induced peripheral neuropathy. *Pain* 2017; 158(6):1126–37. <https://doi.org/10.1097/j.pain.0000000000000893>
33. Sivapackiam J, Kabra S, Speidel S et al. ⁶⁸Ga-Galmydar: a PET imaging tracer for noninvasive detection of doxorubicin-induced cardiotoxicity. *PLoS One* 2019; 14(5):e0215579. <https://doi.org/10.1371/journal.pone.0215579>
34. Jablonski KA, Amici SA, Webb LM et al. Novel markers to delineate murine M1 and M2 macrophages. *PLoS One* 2015; 10(12):e0145342. <https://doi.org/10.1371/journal.pone.0145342>
35. Reichling DB, Levine JD. Critical role of nociceptor plasticity in chronic pain. *Trends Neurosci* 2009; 32(12):611–8. <https://doi.org/10.1016/j.tins.2009.07.007>
36. Lopes AH, Silva RL, Fonseca MD et al. Molecular basis of carrageenan-induced cytokines production in macrophages. *Cell Commun Signal* 2020; 18(1):141. <https://doi.org/10.1186/s12964-020-00621-x>
37. Coll RC, Robertson AAB, Chae JJ et al. A small-molecule inhibitor of the NLRP3 inflammasome for the treatment of inflammatory diseases. *Nat Med* 2015; 21(3):248–55. <https://doi.org/10.1038/nm.3806>
38. Thomas MJ, Guillemin F, Neogi T. Osteoarthritis flares. *Clin Geriatr Med* 2022; 38(2):239–57. <https://doi.org/10.1016/j.cger.2021.11.001>
39. Ueki H, Wang IH, Zhao D et al. Multicolor two-photon imaging of in vivo cellular pathophysiology upon influenza virus infection using the two-photon IMPRESS. *Nat Protoc* 2020; 15(3):1041–65. <https://doi.org/10.1038/s41596-019-0275-y>
40. Guo C, Fu R, Wang S et al. NLRP3 inflammasome activation contributes to the pathogenesis of rheumatoid arthritis. *Clin Exp Immunol* 2018; 194(2):231–43. <https://doi.org/10.1111/cei.13167>
41. Futani H, Okayama A, Matsui K et al. Relation between interleukin-18 and PGE2 in synovial fluid of osteoarthritis: a potential therapeutic target of cartilage degradation. *J Immunother* 2002; 25(1):S61–4. <https://doi.org/10.1097/00002371-200203001-00009>
42. Sun Q, Zhang Y, Ding Y et al. Inhibition of PGE2 in subchondral bone attenuates osteoarthritis. *Cells* 2022; 11(17):2760. <https://doi.org/10.3390/cells11172760>
43. Dubin AE, Patapoutian AN. The sensors of the pain pathway. *J Clin Invest* 2010; 120(11):3760–72. <https://doi.org/10.1172/JCI42843>
44. Xiang HC, Lin L-X, Hu X-F et al. AMPK activation attenuates inflammatory pain through inhibiting NF- κ B activation and IL-1 β expression. *J Neuroinflammation* 2019; 16(1):34. <https://doi.org/10.1186/s12974-019-1411-x>
45. Pivovarova NB, Hongpaisan J, Andrews SB et al. Depolarization-induced mitochondrial Ca accumulation in sympathetic neurons: spatial and temporal characteristics. *J Neurosci Off J Soc Neurosci* 1999; 19(15):6372–84. <https://doi.org/10.1523/JNEUROSCI.19-15-06372.1999>
46. Brookes PS, Yoon Y, Robotham JL et al. Calcium, ATP, and ROS: a mitochondrial love-hate triangle. *Am J Physiol Physiol* 2004; 287(4):C817–33. <https://doi.org/10.1152/ajpcell.00139.2004>
47. Solleiro-Villavicencio H, Rivas-Arancibia S. Effect of chronic oxidative stress on neuroinflammatory response mediated by CD4+T cells in neurodegenerative diseases. *Front Cell Neurosci* 2018; 12:114. <https://doi.org/10.3389/fncel.2018.00114>
48. Wang Y, Hu H, Yin J et al. TLR4 participates in sympathetic hyperactivity Post-MI in the PVN by regulating NF- κ B pathway and ROS production. *Redox Biol* 2019; 24:101186. <https://doi.org/10.1016/j.redox.2019.101186>
49. Marchi S, Guilbaud E, Tait SWG et al. Mitochondrial control of inflammation. *Nat Rev Immunol* 2022; 23(3):159–73. <https://doi.org/10.1038/s41577-022-00760-x>
50. Chen PY, Yen JC, Liu TT et al. Neuronal NLRP3 inflammasome mediates spreading depolarization-evoked trigeminovascular activation. *Brain* 2023; 146(7):2989–3002. <https://doi.org/10.1093/brain/awad045>
51. Xu L, Wang Q, Jiang W et al. MiR-34c Ameliorates neuropathic pain by targeting NLRP3 in a mouse model of chronic constriction injury. *Neuroscience* 2019; 399:125–34. <https://doi.org/10.1016/j.neuroscience.2018.12.030>
52. Derangula K, Javalegar M, Kumar Arruri V et al. Probulcol attenuates NF- κ B/NLRP3 signalling and augments Nrf-2 mediated antioxidant defence in nerve injury induced neuropathic pain. *Int Immunopharmacol* 2022; 102:108397. <https://doi.org/10.1016/j.intimp.2021.108397>
53. Tonkin RS, Bowles C, Perera CJ et al. Attenuation of mechanical pain hypersensitivity by treatment with Peptide5, a connexin-43 mimetic peptide, involves inhibition of NLRP3 inflammasome in nerve-injured mice. *Exp Neurol* 2018; 300:1–12. <https://doi.org/10.1016/j.expneurol.2017.10.016>
54. Huang A, Ji L, Huang Y et al. miR-185-5p alleviates CCI-induced neuropathic pain by repressing NLRP3 inflammasome through dual targeting MyD88 and CXCR4. *Int Immunopharmacol* 2022; 104:108508. <https://doi.org/10.1016/j.intimp.2021.108508>
55. Chen SP, Zhou Y-Q, Wang X-M et al. Pharmacological inhibition of the NLRP3 inflammasome as a potential target for cancer-induced bone pain. *Pharmacol Res* 2019; 147:104339. <https://doi.org/10.1016/j.phrs.2019.104339>
56. Chen R, Yin C, Fang J et al. The NLRP3 inflammasome: an emerging therapeutic target for chronic pain. *J Neuroinflammation* 2021; 18(1):84. <https://doi.org/10.1186/s12974-021-02131-0>
57. Pan Z, Shan Q, Gu P et al. miRNA-23a/CXCR4 regulates neuropathic pain via directly targeting TXNIP/NLRP3 inflammasome axis. *J Neuroinflammation* 2018; 15(1):29. <https://doi.org/10.1186/s12974-018-1073-0>
58. Cowie AM, Menzel AD, O'Hara C et al. NOD-like receptor protein 3 inflammasome drives postoperative mechanical pain in a sex-dependent manner. *Pain* 2019; 160(8):1794–816. <https://doi.org/10.1097/j.pain.0000000000001555>
59. Huang J, Gandini MA, Chen L et al. Hyperactivity of innate immunity triggers pain via TLR2-IL-33-mediated neuroimmune crosstalk. *Cell Rep* 2020; 33(1):108233. <https://doi.org/10.1016/j.celrep.2020.108233>
60. Wahlman C, Doyle TM, Little JW et al. Chemotherapy-induced pain is promoted by enhanced spinal adenosine kinase levels through astrocyte-dependent mechanisms. *Pain* 2018; 159(6):1025–34. <https://doi.org/10.1097/j.pain.0000000000001177>
61. Jung M, Dourado M, Maksymetz J et al. Cross-species transcriptomic atlas of dorsal root ganglia reveals species-specific programs for sensory function. *Nat Commun* 2023; 14(1):366. <https://doi.org/10.1038/s41467-023-36014-0>
62. North RY, Li Y, Ray P et al. Electrophysiological and transcriptomic correlates of neuropathic pain in human dorsal root ganglion neurons. *Brain* 2019; 142(5):1215–26. <https://doi.org/10.1093/brain/awz063>

63. Molnar V, Matišić V, Kodvanj I et al. Cytokines and chemokines involved in osteoarthritis pathogenesis. *Int J Mol Sci* 2021; 22(17):9208. <https://doi.org/10.3390/ijms22179208>
64. Sachdeva M, Aggarwal A, Sharma R et al. Chronic inflammation during osteoarthritis is associated with an increased expression of CD161 during advanced stage. *Scand J Immunol* 2019; 90(1):e12770. <https://doi.org/10.1111/sji.12770>
65. Molnár K, Nógrádi B, Kristóf R et al. Motoneuronal inflammasome activation triggers excessive neuroinflammation and impedes regeneration after sciatic nerve injury. *J Neuroinflammation* 2022; 19(1):68. <https://doi.org/10.1186/s12974-022-02427-9>
66. Kim HY, Lee I, Chun SW et al. Reactive oxygen species donors increase the responsiveness of dorsal horn neurons and induce mechanical hyperalgesia in rats. *Neural Plast* 2015; 2015:293423. <https://doi.org/10.1155/2015/293423>
67. Kucia M, Bujko K, Thapa A et al. A novel view of the role of prostaglandin E2 (PGE2) in facilitating engraftment of HSPCs by activating the NOX2-ROS-Nlrp3 inflammasome axis to incorporate the CXCR4 receptor into membrane lipid rafts. *Blood* 2020; 136(1):3. <https://doi.org/10.1182/blood-2020-137102>
68. De Corato A, Lisi L, Capuano A et al. Trigeminal satellite cells express functional calcitonin gene-related peptide receptors, whose activation enhances interleukin-1 β pro-inflammatory effects. *J Neuroimmunol* 2011; 237(1–2):39–46. <https://doi.org/10.1016/j.jneuroim.2011.05.013>
69. González-Reyes S, Orozco-Ibarra M, Guzmán-Beltrán S et al. Neuroprotective role of heme-oxygenase 1 against iodoacetate-induced toxicity in rat cerebellar granule neurons: role of bilirubin. *Free Radic Res* 2009; 43(3):214–23. <https://doi.org/10.1080/10715760802676670>
70. Glasson SS, Blanchet TJ, Morris EA. The surgical destabilization of the medial meniscus (DMM) model of osteoarthritis in the 129/SvEv mouse. *Osteoarthritis Cartilage* 2007; 15(9):1061–9. <https://doi.org/10.1016/j.joca.2007.03.006>
71. Zhang H, Tang Y, Tao J. Sex-related overactivation of NLRP3 inflammasome increases lethality of the male COVID-19 patients. *Front Mol Biosci* 2021; 8:671363. <https://doi.org/10.3389/fmolb.2021.671363>
72. Wu X, Cakmak S, Wortmann M et al. Sex- and disease-specific inflammasome signatures in circulating blood leukocytes of patients with abdominal aortic aneurysm. *Mol Med* 2016; 22:505–18. <https://doi.org/10.2119/molmed.2016.00035>
73. Di Florio DN, Sin J, Coronado MJ et al. Sex differences in inflammation, redox biology, mitochondria and autoimmunity. *Redox Biol* 2020; 31:101482. <https://doi.org/10.1016/j.redox.2020.101482>
74. Falk S, Uldall M, Appel C et al. Influence of sex differences on the progression of cancer-induced bone pain. *Anticancer Res* 2013; 33(5):1963–9.
75. Muralidharan A, Sotocinal SG, Yousefpour N et al. Long-term male-specific chronic pain via telomere- and p53-mediated spinal cord cellular senescence. *J Clin Invest* 2022; 132(8):e151817. <https://doi.org/10.1172/JCI151817>
76. Mapplebeck JCS, Dalgarno R, Tu YS et al. Microglial P2X4R-evoked pain hypersensitivity is sexually dimorphic in rats. *Pain* 2018; 159(9):1752–63. <https://doi.org/10.1097/j.pain.0000000000001265>
77. Rosen S, Ham B, Mogil JS. Sex differences in neuroimmunity and pain. *J Neurosci Res* 2017; 95(1–2):500–8. <https://doi.org/10.1002/jnr.23831>
78. Mogil JS. Sex differences in pain and pain inhibition: multiple explanations of a controversial phenomenon. *Nat Rev Neurosci* 2012; 13(12):859–66. <https://doi.org/10.1038/nrn3360>
79. Sorge RE, LaCroix-Fralish ML, Tuttle AH et al. Spinal cord Toll-like receptor 4 mediates inflammatory and neuropathic hypersensitivity in male but not female mice. *J Neurosci Off J Soc Neurosci* 2011; 31(43):15450–4. <https://doi.org/10.1523/JNEUROSCI.3859-11.2011>
80. Sorge RE, Mapplebeck JCS, Rosen S et al. Different immune cells mediate mechanical pain hypersensitivity in male and female mice. *Nat Neurosci* 2015; 18(8):1081–3. <https://doi.org/10.1038/nn.4053>
81. Liu L, Karagoz H, Herneisey M et al. Sex differences revealed in a mouse CFA inflammation model with macrophage targeted nanotheranostics. *Theranostics* 2020; 10(4):1694–707. <https://doi.org/10.7150/thno.41309>
82. Yu X, Liu H, Hamel KA et al. Dorsal root ganglion macrophages contribute to both the initiation and persistence of neuropathic pain. *Nat Commun* 2020; 11(1):264. <https://doi.org/10.1038/s41467-019-13839-2>
83. Cepeda MS, Carr DB. Women experience more pain and require more morphine than men to achieve a similar degree of analgesia. *Anesth Analg* 2003; 97(5):1464–8. <https://doi.org/10.1213/01.ANE.0000080153.36643.83>
84. Aubrun F, Salvi N, Coriat P et al. Sex- and age-related differences in morphine requirements for postoperative pain relief. *Anesthesiology* 2005; 103(1):156–60. <https://doi.org/10.1097/0000542-200507000-00023>
85. Klück V, Jansen TLTA, Janssen M et al. Dapansutrile, an oral selective NLRP3 inflammasome inhibitor, for treatment of gout flares: an open-label, dose-adaptive, proof-of-concept, phase 2a trial. *Lancet Rheumatol* 2020; 2(5):e270–80. [https://doi.org/10.1016/s2665-9913\(20\)30065-5](https://doi.org/10.1016/s2665-9913(20)30065-5)
86. Atemnkeng Ntam V, Klein A, Horneff G. Safety and efficacy of anakinra as first-line or second-line therapy for systemic onset juvenile idiopathic arthritis - data from the German BIKER registry. *Expert Opin Drug Saf* 2021; 20(1):93–100. <https://doi.org/10.1080/14740338.2021.1843631>
87. Szturz P, Sedivá A, Zurek M et al. Anakinra treatment in Schnitzler syndrome - results of the first retrospective multicenter study in six patients from the Czech Republic. *Klin Onkol* 2014; 27(2):111–26. <https://doi.org/10.14735/amko2014111>